Taylor & Francis
Taylor & Francis Group

Vehicle System Dynamics
International Journal of Vehicle Mechanics and Mobility

ISSN: 0042-3114 (Print) 1744-5159 (Online) Journal homepage: http://www.tandfonline.com/loi/nvsd20

Sideslip estimation for articulated heavy vehicles at the limits of adhesion

Graeme Morrison & David Cebon

To cite this article: Graeme Morrison & David Cebon (2016) Sideslip estimation for articulated heavy vehicles at the limits of adhesion, Vehicle System Dynamics, 54:11, 1601-1628, DOI: 10.1080/00423114.2016.1223326

To link to this article: http://dx.doi.org/10.1080/00423114.2016.1223326

Published online: 02 Sep 2016.

VEHICLE SYSTEM DYNAMICS, 2016
VOL. 54, NO. 11, 1601–1628
http://dx.doi.org/10.1080/00423114.2016.1223326

Sideslip estimation for articulated heavy vehicles at the limits of adhesion*

Graeme Morrison and David Cebon

Department of Engineering, University of Cambridge, Cambridge, UK

ABSTRACT

Various active safety systems proposed for articulated heavy goods vehicles (HGVs) require an accurate estimate of vehicle sideslip angle. However in contrast to passenger cars, there has been minimal published research on sideslip estimation for articulated HGVs. State-of-the-art observers, which rely on linear vehicle models, perform poorly when manoeuvring near the limits of tyre adhesion. This paper investigates three nonlinear Kalman filters (KFs) for estimating the tractor sideslip angle of a tractor–semitrailer. These are compared to the current state-of-the-art, through computer simulations and vehicle test data. An unscented KF using a 5 degrees-of-freedom single-track vehicle model with linear adaptive tyres is found to substantially outperform the state-of-the-art linear KF across a range of test manoeuvres on different surfaces, both at constant speed and during emergency braking. Robustness of the observer to parameter uncertainty is also demonstrated.

ARTICLE HISTORY
Received 14 March 2016
Revised 16 July 2016
Accepted 5 August 2016

KEYWORDS
Sideslip estimation; state observer; heavy goods vehicle; extended Kalman filter; unscented Kalman filter; linear adaptive

Nomenclature

a_{yi}	lateral acceleration at CoG of vehicle unit i
g	gravitational acceleration
$h_{i\mathrm{cr}}$	vertical distance from roll axis to hitch point on vehicle unit i
$h_{i\mathrm{sr}}$	vertical distance from roll axis to sprung mass CoG on vehicle unit i
$l_{1\mathrm{f}}$	longitudinal distance from front axle to whole mass CoG on tractor
$l_{1\mathrm{r}}$	longitudinal distance from rear axle to whole mass CoG on tractor
$l_{2\mathrm{aa}}$	longitudinal semitrailer axle spacing
$l_{2\mathrm{r}}$	longitudinal distance from middle axle to whole mass CoG on semitrailer
l_{ic}	longitudinal distance from hitch point to whole mass CoG on vehicle unit i
m_i	whole mass of vehicle unit i
m_{is}	sprung mass of vehicle unit i
u_i	longitudinal velocity of vehicle unit i
u_{w}	planar velocity of wheel
C_1	lateral tyre stiffness
C_2	longitudinal tyre stiffness

CONTACT David Cebon dc@eng.cam.ac.uk

*Data supporting this research can be accessed at http://dx.doi.org/10.17863/CAM.1234

C_i^* composite roll damping of vehicle unit i
$C_{\alpha,n}$ total cornering stiffness of axle n
$C_{\alpha(0),n}$ constant nominal cornering stiffness of axle n
$\Delta C_{\alpha,n}$ adaptive cornering stiffness of axle n
$F_{y,n}$ lateral tyre force at axle n
$F_{zs,n}$ static normal load on axle n
I_{isxx} sprung mass roll moment of inertia of vehicle unit i
I_{isxz} sprung mass yaw–roll product of inertia of vehicle unit i
I_{izz} whole mass yaw moment of inertia of vehicle unit i
K_{12} hitch point roll stiffness
K_i^* composite roll stiffness of vehicle unit i
$N_{\mathrm{a},n}$ number of tyres on axle n
V_{f} Fancher tyre model 'friction shaping velocity'
α_n tyre sideslip angle at axle n
β_i sideslip angle at CoG of vehicle unit i
$\delta_{1\mathrm{f}}$ tractor front axle road–wheel steering angle
λ_n mean longitudinal wheel slip on axle n
μ_0 Fancher tyre model static coefficient of friction
μ_{f} Fancher tyre model sliding coefficient of friction
ϕ_i roll angle of vehicle unit i
ψ_i yaw angle of vehicle unit i

1. Introduction

Sideslip angle information is required by advanced driver assistance systems for passenger cars and several active safety technologies proposed for articulated heavy goods vehicles (HGVs), including active trailer steering,[1–3] electronic stability control [4,5] and emergency braking control.[6–8] Sideslip cannot be measured directly using standard inexpensive sensors, therefore it must be estimated based on other available sensor information.

There is a wealth of literature regarding estimation of sideslip angle at the centre of gravity (CoG) of passenger cars.[9–18] When the vehicle manoeuvres well below the limits of tyre adhesion, observers based around linear vehicle models with linear tyre behaviour are sufficient.[9,12] Adaptive or nonlinear tyre models must be adopted if the observer is to function when the limits of tyre adhesion are approached (e.g. on low-friction surfaces or under conditions of high lateral or longitudinal acceleration).[10–12]

In contrast, literature concerning sideslip estimation for HGVs is scarce. The state-of-the-art for articulated HGVs is the linear Kalman filter (KF) designed by Cheng and Cebon,[19] based around a linear 5 degrees-of-freedom (DoF) yaw–roll vehicle model with linear tyre behaviour. In full-scale vehicle tests with a tractor–semitrailer on high-friction surfaces (i.e. manoeuvring well below the limits of tyre adhesion), the observer produced accurate sideslip and roll angle estimates for both vehicle units. However, it has been demonstrated that the observer's performance breaks down as the limits of adhesion are approached.[20] HGVs are less likely to encounter such conditions than passenger cars, since on a dry road surface they will tend to rollover long before the onset of nonlinear tyre behaviour. Nonetheless, HGV tyres may still reach the limits of adhesion if either the

tyre–road friction coefficient is low or they are saturated longitudinally by heavy braking. Ma et al. [21] recently published simulation results for an observer to estimate the longitudinal and lateral velocities (from which sideslip angle can be calculated) of rigid HGVs on roads of unknown slope angle. However, their observer requires an accurate model of the vehicle's tyre characteristics and accurate knowledge of the tyre–road friction conditions.

This paper investigates nonlinear sideslip observers for a tractor–semitrailer, to improve sideslip estimation at the limits of adhesion. Specifically, sideslip at the tractor unit's CoG is considered, since trailer sideslip angle can be calculated by combining the tractor sideslip estimate with other vehicle states which are easily measured. In Section 2, Cheng and Cebon's linear KF is introduced. This is used as a baseline for comparison throughout the paper. In Section 3, three nonlinear sideslip observers are presented. Simulations are then used in Section 4 to explore the performance of the observers in constant speed manoeuvring on both high- and low-friction surfaces. In Section 5, the observers are applied in post-processing to data from full-scale vehicle tests. Performance in both constant speed and emergency braking manoeuvres is evaluated. Finally in Section 6, sensitivity to parameter uncertainty is considered.

2. Cheng and Cebon's linear KF

2.1. 5 DoF yaw–roll model

Cheng and Cebon's linear KF [19] is based around the 5 DoF yaw–roll vehicle model in Figure 1. The model is single-track and has constant forward speed u_1. Subscripts '1' and '2' denote the tractor and semitrailer units, respectively. Each has 3 DoFs (sideslip angle β, yaw rate $\dot{\psi}$ and roll angle ϕ) and they are kinematically constrained in the lateral direction at the fifth wheel coupling. Articulation angle, roll angles and steering angle ($\delta_{1\mathrm{f}}$) are assumed small. The chassis of each vehicle unit is rigid and pitch and bounce motions are ignored. The unsprung masses are assumed not to roll relative to the ground plane, which is taken to be flat and smooth.

The sums of lateral tyre forces at the tractor front and rear and trailer front, middle and rear axles are denoted $F_{y,1\mathrm{f}}$, $F_{y,1\mathrm{r}}$, $F_{y,2\mathrm{f}}$, $F_{y,2m}$ and $F_{y,2\mathrm{r}}$, respectively. These obey the linear lateral tyre model:

$$F_{y,n} = -C_{\alpha,n}\alpha_n, \tag{1}$$

where α_n is the sideslip angle of the single-track tyre at axle n and $C_{\alpha,n}$ is a constant cornering stiffness. The equations of motion (see [19]) can be arranged into the state-space form:

$$\dot{\boldsymbol{x}} = \boldsymbol{A}(u_1)\boldsymbol{x} + \boldsymbol{B}(u_1)\delta_{1\mathrm{f}}, \tag{2}$$

where $\boldsymbol{x} = \begin{bmatrix}\phi_1 & \dot{\phi}_1 & \beta_1 & \dot{\psi}_1 & \phi_2 & \dot{\phi}_2 & \beta_2 & \dot{\psi}_2\end{bmatrix}^{\mathrm{T}}$ and the matrices $\boldsymbol{A}$ and $\boldsymbol{B}$ are given in Appendix 1.

2.2. Sensor measurements and filter

The KF corrects the state predictions of the vehicle model by comparing the model outputs to a set of corresponding sensor measurements. Cheng and Cebon [19] used only the yaw and roll rates of each vehicle unit as outputs, measured on the vehicle by gyroscopes. In this

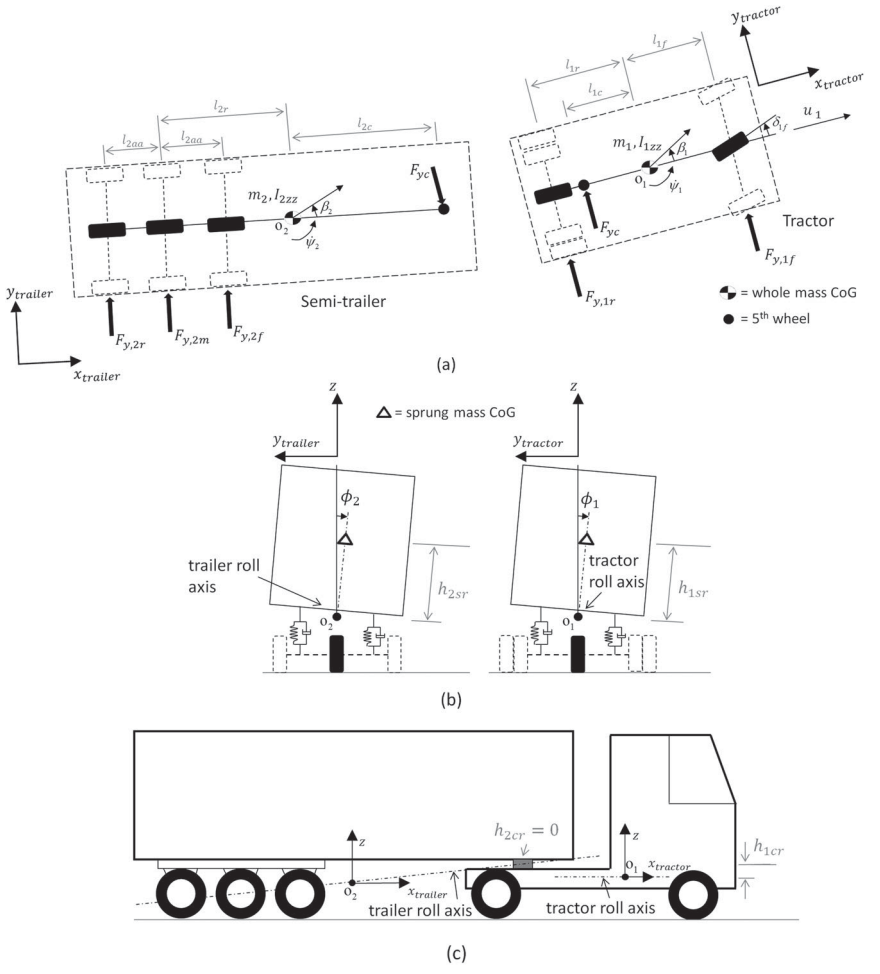

Figure 1. Cheng and Cebon's linear, single-track 5 DoF yaw–roll model.[19]

study, the lateral accelerations a_{y1} and a_{y2} at the tractor and semitrailer CoGs, respectively, which can be measured by lateral accelerometers, were also included. The output vector is therefore:

$$\boldsymbol{z} = \begin{bmatrix} a_{y1} & \dot{\psi}_1 & \dot{\phi}_1 & a_{y2} & \dot{\psi}_2 & \dot{\phi}_2 \end{bmatrix}^{\mathrm{T}} = \boldsymbol{C}(u_1)\boldsymbol{x} + \boldsymbol{D}(u_1)\delta_{1\mathrm{f}}, \tag{3}$$

where $\boldsymbol{C}$ and $\boldsymbol{D}$ are given in Appendix 1. The lateral acceleration measurements have a negligible effect on the performance of the KF. They were included for fair comparison to the nonlinear filters designed later in the paper, which use the same set of sensors. Note that in addition to the six model output measurements, sensors are also required to measure tractor steering angle $\delta_{1\mathrm{f}}$ as the model input and forward vehicle speed u_1 in order to form the state-space matrices.

3. Nonlinear observers

The following sections describe three nonlinear alternatives to Cheng and Cebon's observer, each based around the same 5 DoF yaw–roll vehicle model but augmented with either a linear adaptive or nonlinear tyre model.

In an earlier paper,[20] the same observers were investigated using a 3 DoF yaw–plane only version of the vehicle model. Yaw–plane models have been successfully used in sideslip observers for passenger cars.[9,11,12] However, HGVs experience more substantial body roll, which corrupts measurements of lateral acceleration with tangential and gravitational components. The observers therefore performed poorly using the 3 DoF model. Their performance is substantially improved using the 5 DoF yaw–roll model, since the effects of body roll can be explicitly accounted for in the measurement model (Equation (3)).

3.1. Linear adaptive extended Kalman filter

Baffet et al. [12] demonstrated that an extended Kalman filter (EKF), using a single-track vehicle model augmented with a linear adaptive tyre model, could accurately estimate sideslip of a passenger car in a range of friction conditions and manoeuvres. Therefore, a similar linear adaptive EKF (LAEKF) was investigated in this study, adapted for a tractor–semitrailer.

For the LAEKF, the lateral tyre force at axle n continues to be given by Equation (1), but with cornering stiffness $C_{\alpha,n}$ given by

$$C_{\alpha,n} = C_{\alpha(0),n} + \Delta C_{\alpha,n}, \tag{4}$$

where $C_{\alpha(0),n}$ is a constant 'nominal' value and $\Delta C_{\alpha,n}$ is an adaptive value. The vehicle model is augmented with the three new adaptive stiffness states $\Delta C_{\alpha,1\mathrm{f}}$, $\Delta C_{\alpha,1\mathrm{r}}$ and $\Delta C_{\alpha,2}$ (where $C_{\alpha,2} = C_{\alpha,2\mathrm{f}} + C_{\alpha,2m} + C_{\alpha,2\mathrm{r}}$), giving:

$$\dot{\boldsymbol{x}}_{LA} = \boldsymbol{A}_{\boldsymbol{LA}}(\boldsymbol{x}_{\boldsymbol{LA}}, u_1)\boldsymbol{x}_{\boldsymbol{LA}} + \boldsymbol{B}_{\boldsymbol{LA}}(\boldsymbol{x}_{\boldsymbol{LA}}, u_1)\delta_{1\mathrm{f}} \tag{5}$$

where

$$\boldsymbol{x}_{\boldsymbol{LA}} = \begin{bmatrix}\boldsymbol{x}^{\mathrm{T}} & \Delta C_{\alpha,1\mathrm{f}} & \Delta C_{\alpha,1\mathrm{r}} & \Delta C_{\alpha,2}\end{bmatrix}^{\mathrm{T}},$$

$$\boldsymbol{A}_{\boldsymbol{LA}}(\boldsymbol{x}_{\boldsymbol{LA}}, u_1) = \begin{bmatrix}\boldsymbol{A}(\boldsymbol{x}_{\boldsymbol{LA}}, u_1) & \begin{matrix}0\\0\end{matrix}\\ \begin{matrix}0 & 0\end{matrix} & \begin{matrix}0\\0\end{matrix}\end{bmatrix}, \quad \boldsymbol{B}_{\boldsymbol{LA}}(\boldsymbol{x}_{\boldsymbol{LA}}, u_1) = \begin{bmatrix}\boldsymbol{B}(\boldsymbol{x}_{\boldsymbol{LA}}, u_1)^{\mathrm{T}} & 0 & 0 & 0\end{bmatrix}^{\mathrm{T}}.$$

The model outputs and sensor measurements are the same as for the linear KF, given in Equation (3). Figure 2 illustrates how the adaptive cornering stiffness enables lateral forces to be correctly predicted even in the nonlinear operating region of the tyres.

With the three augmented states, the model is nonlinear. The EKF is the most common technique for Kalman filtering with nonlinear models [22] and is considered the industry standard approach to inertial navigation.[23] It essentially linearises the model about the current state estimate at each sampling step, then applies the standard KF.

3.2. Linear adaptive unscented Kalman filter

The EKF can suffer from a number of problems. Julier and Uhlmann [24] noted that it is 'difficult to implement ... and only reliable for systems which are almost linear on the

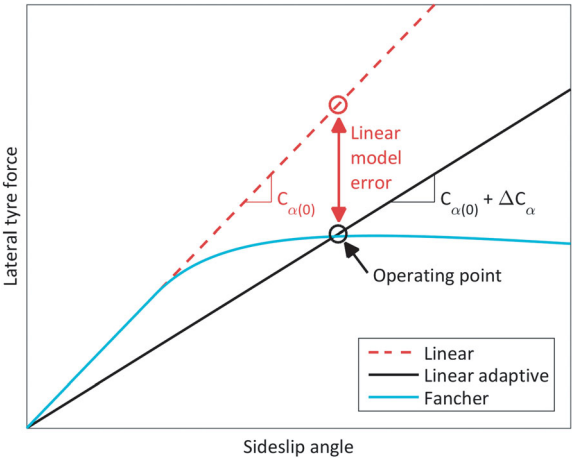

Figure 2. Comparison of linear, linear adaptive and nonlinear Fancher tyre models.

time scale of the update intervals'. Implementation difficulties stem from the need to calculate Jacobian matrices when linearising the model. In the case of the LAEKF described above, these can be computed analytically. However when this is not the case, they must be calculated through some perturbation method or otherwise. This can add significant computational cost and complexity. Furthermore, if the assumption of local linearity breaks down, the EKF can be unstable.[24]

Julier and Uhlmann [24] proposed the unscented Kalman filter (UKF) as an alternative to the EKF. Instead of linearising the model, the unscented transform (UT) is used to propagate a carefully selected set of sample states or 'sigma points' (distributed about the previous state estimate) through the full nonlinear model. The mean and covariance of the model output can then be statistically evaluated, giving at least third-order accuracy for any nonlinearity.[25] In principle, this is similar to a particle filter, but the UT ensures computational cost comparable to the EKF [25] by only evaluating the model for a small number of sigma points. In fact, because there is no need to calculate Jacobian matrices, the UKF may often compute faster than the EKF for the same model.

Antonov et al. [26] found the UKF to be superior to the EKF when applied to passenger car sideslip observers, using a planar vehicle model incorporating load transfers and a nonlinear tyre model with known parameters. The benefit of using the UKF increased with the size of the integration time step, since larger integration steps caused larger errors to result from the EKF's linearisation.

A linear adaptive UKF (LAUKF) was implemented in this study using the same linear adaptive model as the LAEKF. Details of the UT and the prediction and update equations for the UKF can be found in [24].

3.3. Fancher unscented Kalman filter

The final nonlinear observer, a 'Fancher unscented Kalman filter' (FUKF), uses the Fancher tyre model [27]: a semi-empirical, steady state, combined slip model specifically for HGV tyres. The Fancher model has four inputs (tyre sideslip angle α, longitudinal slip λ, normal

tyre load F_z and in-plane wheel velocity u_w) and five parameters (lateral tyre stiffness C_1, longitudinal tyre stiffness C_2, static friction coefficient μ_0, sliding friction coefficient μ_f and a 'friction shaping velocity' V_f). Figure 2 compares the lateral characteristic of the Fancher model, with zero longitudinal slip, to the linear and linear adaptive models.

For the FUKF, Equation (1) is replaced by

$$F_{y,n} = N_n g_F(\alpha_n, \lambda_n, F_{zs,n}/N_{a,n}, u_1), \tag{6}$$

where g_F denotes the Fancher model for a single tyre, λ_n is the mean longitudinal wheel slip of the tyres of that axle, $F_{zs,n}$ is the static normal axle load and N_n is the number of tyres on that axle.

For the purposes of the observer, the lateral and longitudinal stiffness parameters of the Fancher model are classed as 'vehicle parameters' and assumed to remain constant. The remaining three parameters (μ_0, μ_f and V_f) are classed as 'friction parameters', assumed to be the same for all axles but variable depending on the road conditions. The vehicle model is therefore augmented with these three friction parameters as additional states, giving:

$$\dot{\boldsymbol{x}}_{\boldsymbol{F}} = f_F(\boldsymbol{x}_{\boldsymbol{F}}, \delta_{1f}, u_1, \lambda_{1f}, \lambda_{1r}, \lambda_{2f}, \lambda_{2m}, \lambda_{2r}), \tag{7}$$

where $\boldsymbol{x}_{\boldsymbol{F}} = \begin{bmatrix} \boldsymbol{x}^T & \mu_0 & \mu_f/\mu_0 & V_f \end{bmatrix}^T$ and f_F is the nonlinear function formed by substituting Equation (6) for Equation (1) in the 5 DoF vehicle model. The mean longitudinal slips at each axle are considered as inputs. In constant speed manoeuvring, these are assumed to be zero. During braking or acceleration, it is assumed that there is a measurement or estimate of absolute vehicle speed available. Then longitudinal slips can be calculated by combining this with additional wheel speed sensor measurements. The model outputs and sensor measurements are again the same as the linear KF, LAEKF and LAUKF (Equation (3)).

Unlike the linear adaptive model, Jacobian matrices cannot be calculated analytically when using the Fancher tyre model. For this reason only the UKF, and not the EKF, was implemented for this model.

4. Constant speed simulations

4.1. Simulation set-up

Figure 3 illustrates the simulation set-up in Simulink. A previously validated nonlinear model of a tractor–semitrailer [6,8] was used to simulate the plant. This 16 DoF yaw–roll model is two-track, includes lateral and longitudinal load transfers and uses the nonlinear Fancher truck tyre model.[27] A single preview point driver steering model with proportional-integral-derivative feedback controlled the steering angle of the tractor unit's front axle, in order to track a predefined reference path. Band-limited white noise was added to measurements from the plant model before passing them to the observers, in order to simulate real sensor signals. The variance of the noise added to each signal was based on typical values determined by Cheng,[28] from field test data for an experimental tractor–semitrailer.

Four manoeuvres were simulated in total, all at a constant speed of 88 km/h. These were a 300 m radius J-turn (i.e. a straight-line approach followed by a 300 m constant radius curve) and a 3.5 × 61 m lane change each on a high-friction ($\mu = 0.8$) and low-friction ($\mu = 0.2$) surface.

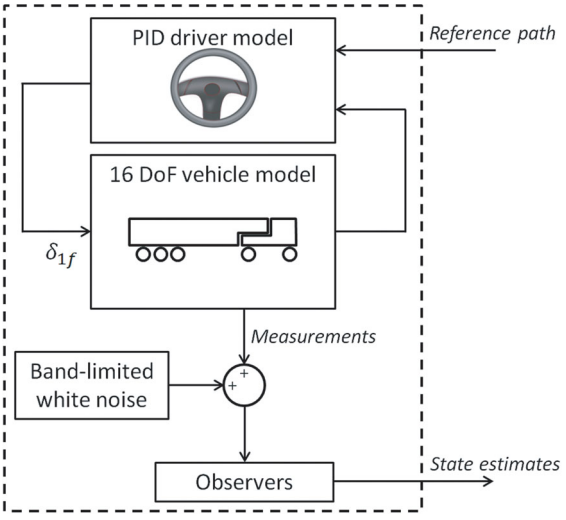

Figure 3. Computer simulation set-up.

All observer state estimates were initialised at zero, with the exception of the friction states in the FUKF which were initialised at $\mu_0 = 0.01$, $\mu_f/\mu_0 = 0.5$ and $V_f = 6\,\text{m/s}$. Following each prediction and update stage of the FUKF, to ensure that the friction state estimates remained within sensible ranges, the estimate of μ_0 was limited to a minimum value of 0.01 and μ_f/μ_0 was limited to between 0.2 and 1.

Nominal cornering stiffness parameters for the KF, LAEKF and LAUKF were set to the sums of lateral stiffness of the tyres on each axle from the plant model, at the static normal wheel loads. Nominal lateral and longitudinal tyre stiffness parameters in the FUKF were set the same as in the plant model at the static normal wheel loads.

The process and measurement noise covariance matrices used for each observer are given in Appendix 2. All four observers were run with a 200 Hz sampling frequency.

4.2. Simulation results

Figure 4 shows results for the J-turn manoeuvre with $\mu = 0.8$. The estimates of the augmented tyre model states are shown for each of the nonlinear observers, in addition to the sideslip estimates. Note that adaptive cornering stiffness estimates are shown only for the LAEKF and LAUKF, since the FUKF does not estimate an adaptive cornering stiffness. Similarly, the estimates of friction coefficients (static μ_0 and sliding μ_f) and friction shaping velocity are shown only for the FUKF, since the linear adaptive tyre model used in the LAEKF and LAUKF does not consider friction.

In this manoeuvre, the vehicle reached an approximately steady state. With the tyres operating well below the limits of adhesion, the linear KF gave an accurate sideslip estimate throughout (Figure 4(a)). The FUKF was equally accurate in the steady state, but produced a small estimation error during the initial transient. The estimate of static friction coefficient μ_0 rose quickly from its initial value of 0.01 at the point of turn-in to the manoeuvre, to a steady value of around 0.4 (Figure 4(d)). This estimate is not expected to correspond to the true static friction coefficient of the road surface, but rather to the

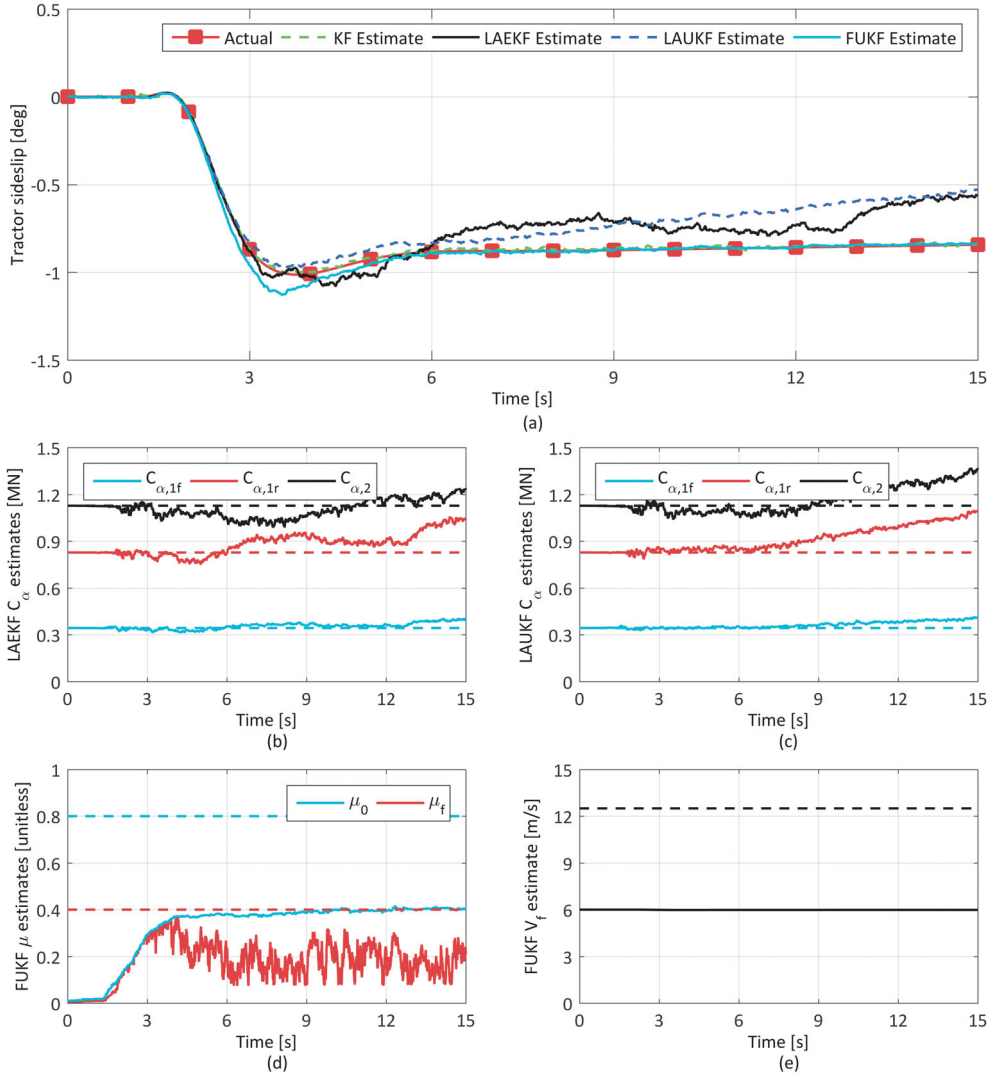

Figure 4. J-turn simulation with $\mu = 0.8$. Estimated: (a) tractor sideslip; (b) cornering stiffness (LAEKF – dashed lines show nominal values); (c) cornering stiffness (LAUKF – dashed lines show nominal values); (d) friction coefficients (FUKF – dashed lines show actual values); and (e) friction shaping velocity (FUKF – dashed line shows actual value).

maximum utilised friction. The utilised friction should be around 0.2 for this manoeuvre, therefore it has been substantially overestimated. This may have contributed to the sideslip estimation error during the initial transient. Since the tyres operated well below the limits of adhesion, the estimates of sliding friction coefficient μ_f and friction shaping velocity V_f are trivial.

The LAEKF and LAUKF sideslip estimates appear qualitatively similar. Both are accurate during the initial transient, but then exhibit a slow divergence during the steady state. The LAEKF estimate has an additional low-frequency oscillation, not present for the LAUKF. The cornering stiffness estimates (Figure 4(b) and 4(c)) appear to

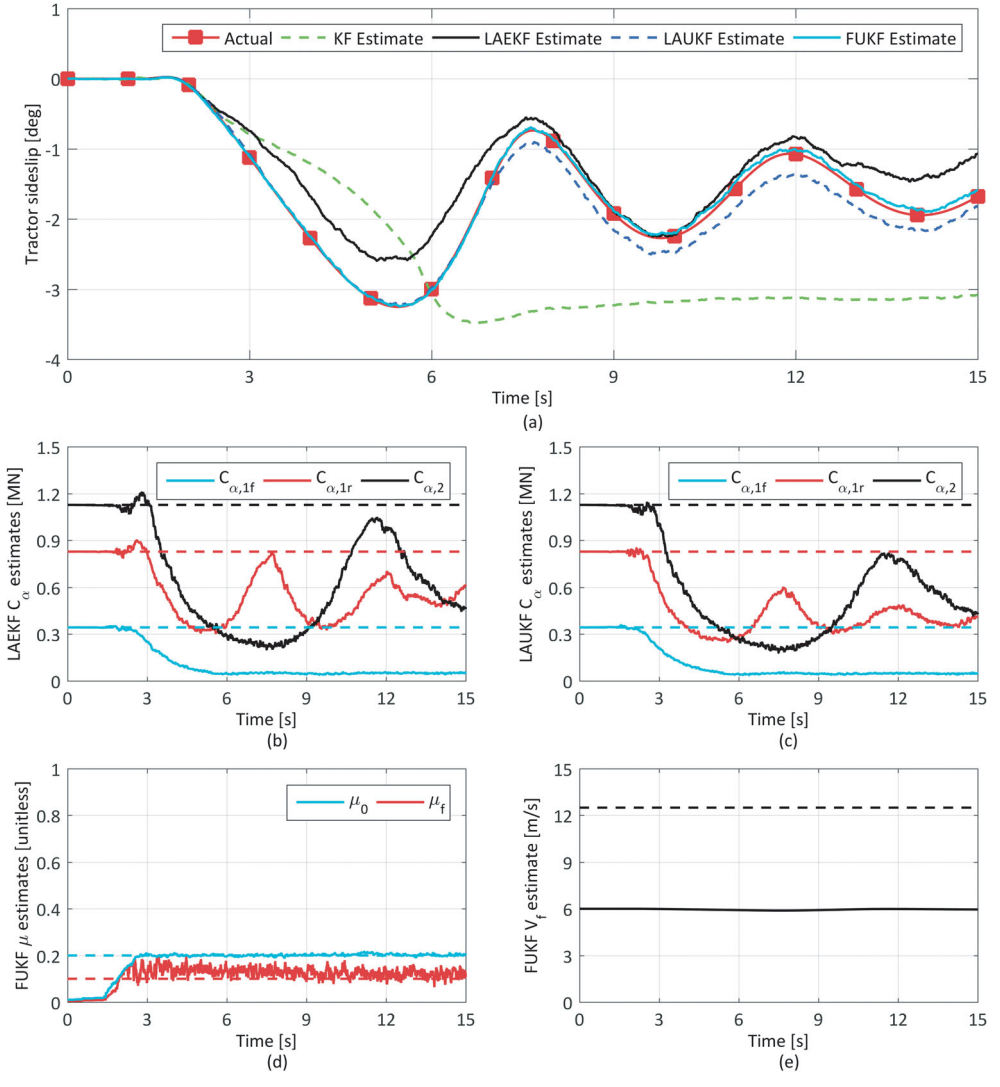

Figure 5. J-turn simulation with $\mu = 0.2$. Estimated: (a) tractor sideslip; (b) cornering stiffness (LAEKF – dashed lines show nominal values); (c) cornering stiffness (LAUKF– dashed lines show nominal values); (d) friction coefficients (FUKF – dashed lines show actual values); and (e) friction shaping velocity (FUKF – dashed line shows actual value).

increase during the steady state to well above their nominal values (seen at the start of the manoeuvre), perhaps suggesting some kind of instability. This will be revisited in Section 4.3.

Results for the J-turn with $\mu = 0.2$ are shown in Figure 5. The utilised friction in this manoeuvre was nominally equal to the available friction, that is, the vehicle was at the limits of adhesion. Therefore, unlike the $\mu = 0.8$ case, a steady state was never reached. The closed-loop combination of vehicle and driver model instead exhibited marginally stable low-frequency oscillations. The linear KF produced large sideslip estimation errors in this case, since the linear tyre assumption no longer held.

The FUKF gave an accurate sideslip estimate throughout the manoeuvre, with the estimate of static friction coefficient rising quickly to the correct value of 0.2 and the sliding friction coefficient estimate also close to the true value. The friction shaping velocity failed to adapt from its initial value, despite the tyres operating well into their nonlinear region. This might suggest that the FUKF model has weak observability.

The LAUKF also performed well in this scenario, matching the FUKF performance early in the manoeuvre, though picking up a small sideslip estimation error peaking around 0.4° at 12 s. Unlike in Figure 4 there was no continued divergence, the error instead decreasing in magnitude again towards the end of the manoeuvre. The LAEKF, despite using the exact same model, gave significantly different results to the LAUKF. The qualitative shape of the sideslip trace was reproduced; however, there were larger errors of around 0.8° both early and late on in the manoeuvre. There were also subtle differences between the cornering stiffness estimates of the LAEKF and LAUKF, though in both cases they were reduced substantially from the nominal values to account for the tyres operating in their nonlinear region.

Figure 6 shows the lane change manoeuvre with $\mu = 0.8$. The sideslip estimates of the linear KF and all three nonlinear observers appear accurate. The cornering stiffness estimates from the LAEKF and LAUKF remained approximately at the nominal values, with no sign of the unstable increase observed in the J-turn at the same friction level.

Figure 7 shows the lane change manoeuvre with $\mu = 0.2$. In this scenario, there were substantial differences between the four observers. With the tyres again operating near the limits of adhesion, the linear KF gave large sideslip errors. The LAEKF performed similarly poorly, however the LAUKF with the same model gave an accurate sideslip estimate throughout. There were subtle differences in the estimated cornering stiffness values between the LAEKF and LAUKF. The FUKF gave similarly accurate sideslip estimates to the LAUKF and again correctly estimated the static friction coefficient at 0.2.

To summarise the results thus far:

(i) the linear KF performed well only when manoeuvring well below the limits of adhesion;
(ii) the FUKF accurately estimated sideslip across the full range of scenarios, both on high and low friction, with the exception of a small error during the initial transient phase of the high-friction J-turn manoeuvre;
(iii) the LAUKF accurately estimated sideslip across the full range of scenarios, both on high and low friction, with the exception of a slow divergence during the steady state of the high-friction J-turn manoeuvre and slightly larger errors than the FUKF during the low-friction J-turn manoeuvre;
(iv) the LAEKF performed poorly in low-friction conditions, despite using the exact same model and tuning as the LAUKF.

The FUKF appears to have the best performance of the four observers. However this should be treated with caution, because the FUKF used the same Fancher tyre model as the plant model. There is no guarantee that this tyre model will remain accurate when applied to a real vehicle. The simpler linear adaptive model is less rigidly constrained since it allows a single tyre parameter to be adapted for each of the three axle groups, rather than three friction parameters to be adapted for the whole vehicle. Therefore, the linear

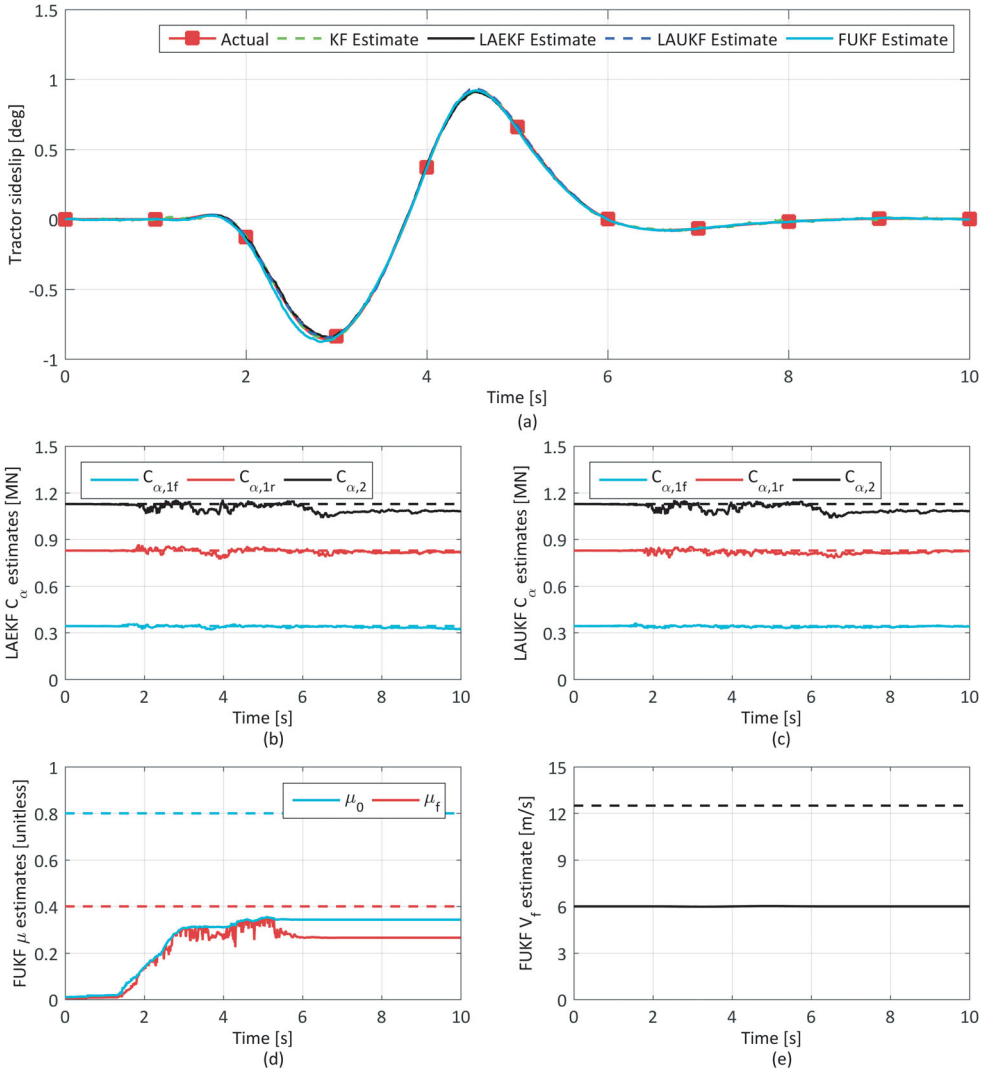

Figure 6. Lane change simulation with $\mu = 0.8$. Estimated: (a) tractor sideslip; (b) cornering stiffness (LAEKF– dashed lines show nominal values); (c) cornering stiffness (LAUKF– dashed lines show nominal values); (d) friction coefficients (FUKF – dashed lines show actual values); and (e) friction shaping velocity (FUKF – dashed line shows actual value).

adaptive model may allow more flexibility to better reproduce a broader range of real tyre characteristics.

The poor performance of the LAEKF, in comparison to the LAUKF, highlights the superiority of the UKF over the EKF in this application. In low-friction conditions, where the tyre characteristics were highly nonlinear, the linearisation of the EKF caused large errors. Therefore of these two observers, only the LAUKF was considered further in this study. However, for the LAUKF the steady-state divergence problem in the high-friction J-turn needs to be addressed.

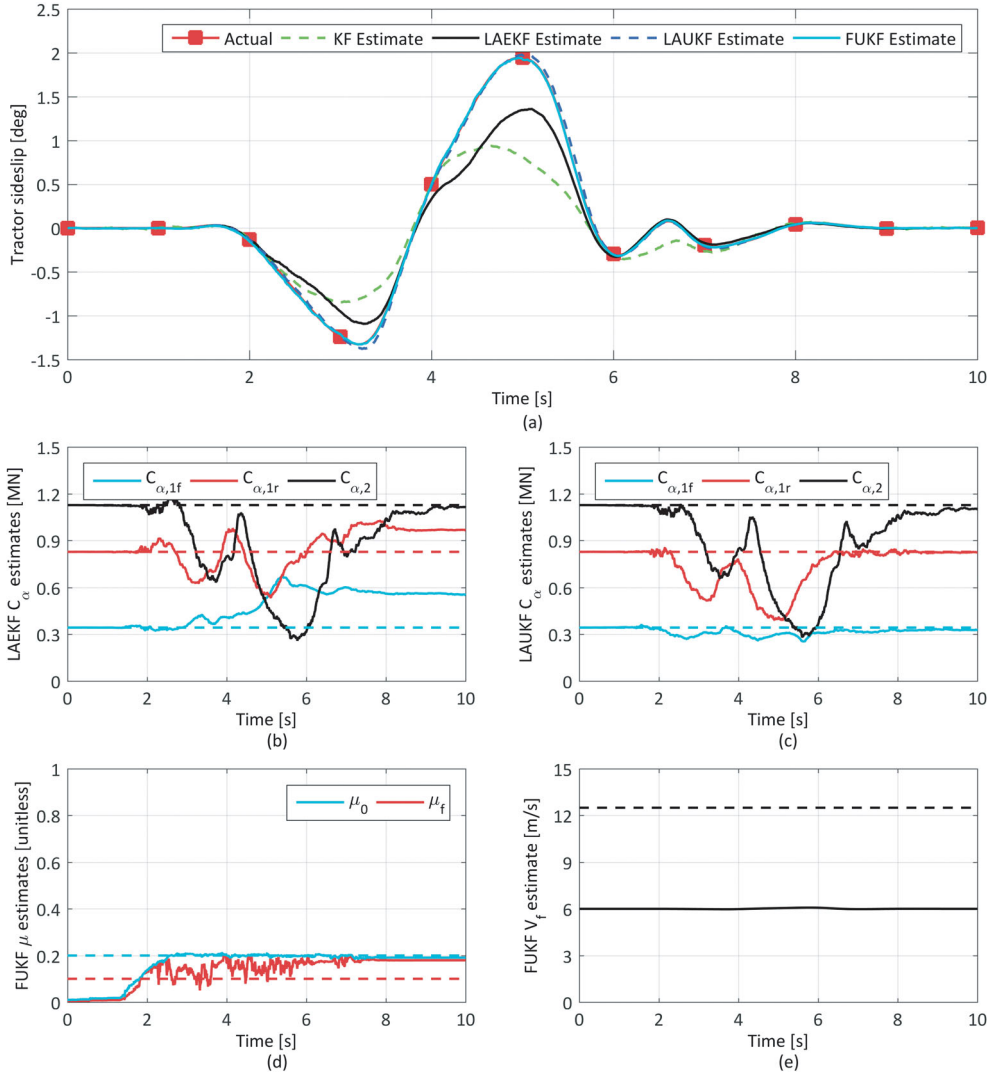

Figure 7. Lane change simulation with $\mu = 0.2$. Estimated: (a) tractor sideslip; (b) cornering stiffness (LAEKF– dashed lines show nominal values); (c) cornering stiffness (LAUKF– dashed lines show nominal values); (d) friction coefficients (FUKF – dashed lines show actual values); and (e) friction shaping velocity (FUKF – dashed line shows actual value).

4.3. Reducing LAUKF divergence in the steady state

Stenlund and Gustafsson [29] noted that when using KFs for parameter estimation, the eigenvalues of the state estimate covariance matrix $\boldsymbol{P}$ can wind up to large values if the system has low excitation. This can cause 'numerical problems' and a high sensitivity to noise. This seems to be relevant to the LAUKF problem: in the steady-state part of the manoeuvre, there is an approximately constant steering input and thus low excitation of the vehicle. Additionally, the LAUKF might be considered to be a parameter estimation algorithm of sorts, since the cornering stiffness parameters are being estimated as additional states.

To investigate this, eigenvalue decomposition in MATLAB was performed on $\boldsymbol{P}$ for each time interval during the high-friction J-turn manoeuvre with the LAUKF. During the steady-state parts of the manoeuvre, the eigenvalues associated with the tractor rear and trailer axles were found to wind up unstably as described by Stenlund and Gustafsson.[29] Additionally, when the high-friction J-turn manoeuvre was repeated with all simulated sensor noise removed, the LAEKF and LAUKF divergence was eliminated. This all suggests that the divergence was caused by wind-up of the eigenvalues of $\boldsymbol{P}$ during times of low excitation, leading to increased sensitivity to noise.

Stenlund and Gustafsson [29] noted a number of possible approaches to alleviating low-excitation wind-up. These will not all be discussed in detail here, but can be found in the following references.[30–34] One such technique – similar to that of Parkum et al. [30] – was tested on the LAUKF. Eigenvalue decomposition was performed on $\boldsymbol{P}$ after every UKF prediction and update stage, and a maximum limit placed on the eigenvalues corresponding to the three cornering stiffness states. $\boldsymbol{P}$ was then recomposed with the limited eigenvalues before being passed to the next prediction or update stage. The maximum limits were set to 5×10^8, 1×10^9 and 1.5×10^9 N^2 on the eigenvalues corresponding to tractor front axle, tractor rear axle and trailer axle-group cornering stiffness states, respectively.

Figure 8 compares the sideslip estimates using the original LAUKF and the LAUKF with limited eigenvalues (LAUKFe) in each of the four constant speed scenarios. In the low-friction J-turn and high- and low-friction lane changes, where the LAUKF performed well before, there was a negligible effect on the results. In the high-friction J-turn, the LAUKFe shows substantially reduced divergence in the steady state compared to the original LAUKF. The limited eigenvalue method therefore appears to have been successful. Further investigation of this or alternative techniques may be necessary to ensure that low-excitation wind-up is always reliably eliminated.

5. Application to field test data

Full-scale vehicle tests were conducted with an instrumented tractor–semitrailer and the linear KF, LAUKF and FUKF were applied to the experimental data in post-processing. Brief descriptions of the test vehicle and experiments are provided later. Refer to [6] for further detail.

5.1. Test vehicle and instrumentation

Figure 9 shows a photograph of the test vehicle and a schematic of the relevant instrumentation installed. The 4×2 Volvo FH12 tractor was supplied by Volvo trucks. This towed an actively steered semitrailer, the axles of which were mechanically locked in the unsteered position. A computer running MATLAB xPC Target was installed inside the tractor cab, to log data from the various sensors and other instrumentation at 100 Hz via CANbus.

Both vehicle units were equipped with the Cambridge Vehicle Dynamics Consortium's (CVDC's) prototype pneumatic slip control braking system, details of which can be found in [35,36]. During emergency braking, this system accurately regulates the slip of each individual wheel to achieve maximum braking force. It has been shown to achieve stopping distance reductions of up to 19% compared to a conventional HGV anti-lock braking

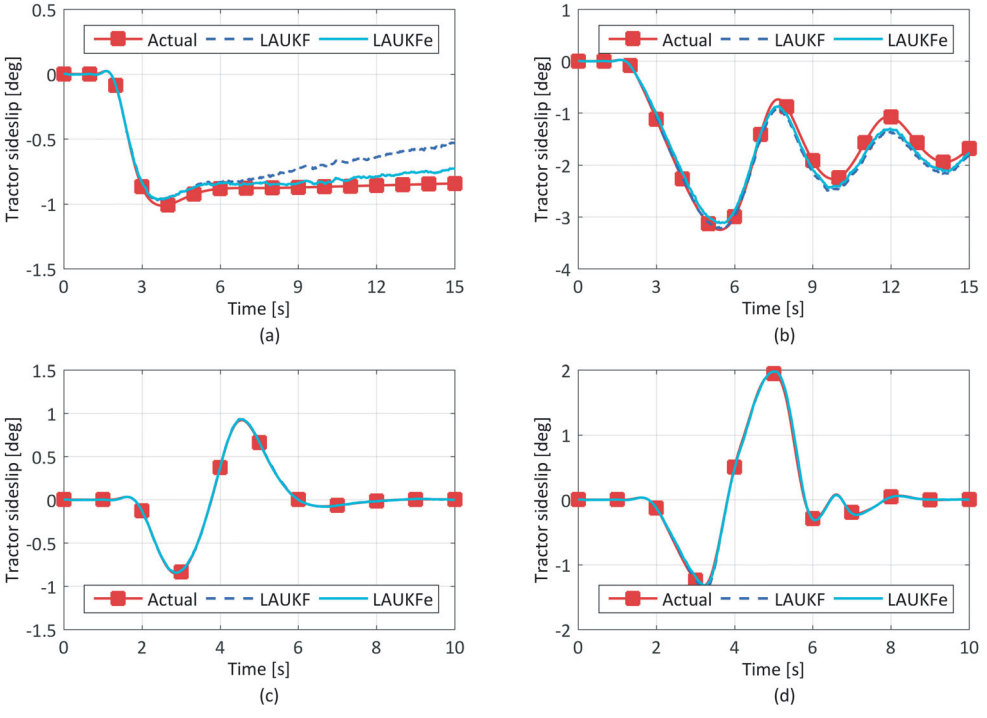

Figure 8. Tractor sideslip estimates using LAUKF and LAUKFe in constant speed simulations, where LAUKFe is the LAUKF with eigenvalues of the state estimate covariance matrix $\boldsymbol{P}$ limited: (a) J-turn, $\mu = 0.8$; (b) J-turn, $\mu = 0.2$; (c) lane change, $\mu = 0.8$; and (d) lane change, $\mu = 0.2$.

system, however in doing so it almost entirely saturates the tyres and leaves very little capacity for lateral forces to be generated.[6–8]

The tractor unit was fitted with an Oxford Technical Solutions RT3022 inertial navigation system. The six-axis inertial sensor and processing unit of the RT3022 was mounted as close as possible to the CoG location of the tractor (determined by weighing the axles when the tractor was decoupled from the trailer). The Global Navigation Satellite System (GNSS) antenna of the RT3022 was mounted on a rigid pylon, in order to give clear access to the sky while still being rigidly fixed to the same body as the inertial sensor unit. A radio connection to a local GNSS base-station was established in order to operate the RT3022 in differential GNSS mode, thereby giving live position data accurate to within 0.02 m.

The raw accelerometer and gyroscope outputs from the RT3022 were used in post-processing as the observer measurements for tractor lateral acceleration, yaw rate and roll rate. The longitudinal velocity measurement was also required as an input to the observers. This information would not typically be available on an everyday vehicle. In constant speed manoeuvring, wheel speed measurements might instead be used to provide vehicle speed information. However, during braking, wheel speeds cannot be relied upon to reflect vehicle speed. Reliable speed estimation algorithms, which have been considered in [10,37–42], would need to be implemented in practice. The CVDC slip control braking system also relies on accurate vehicle speed information, and in these experiments it also used the longitudinal speed measurement from the RT3022. The lateral speed measurement from the

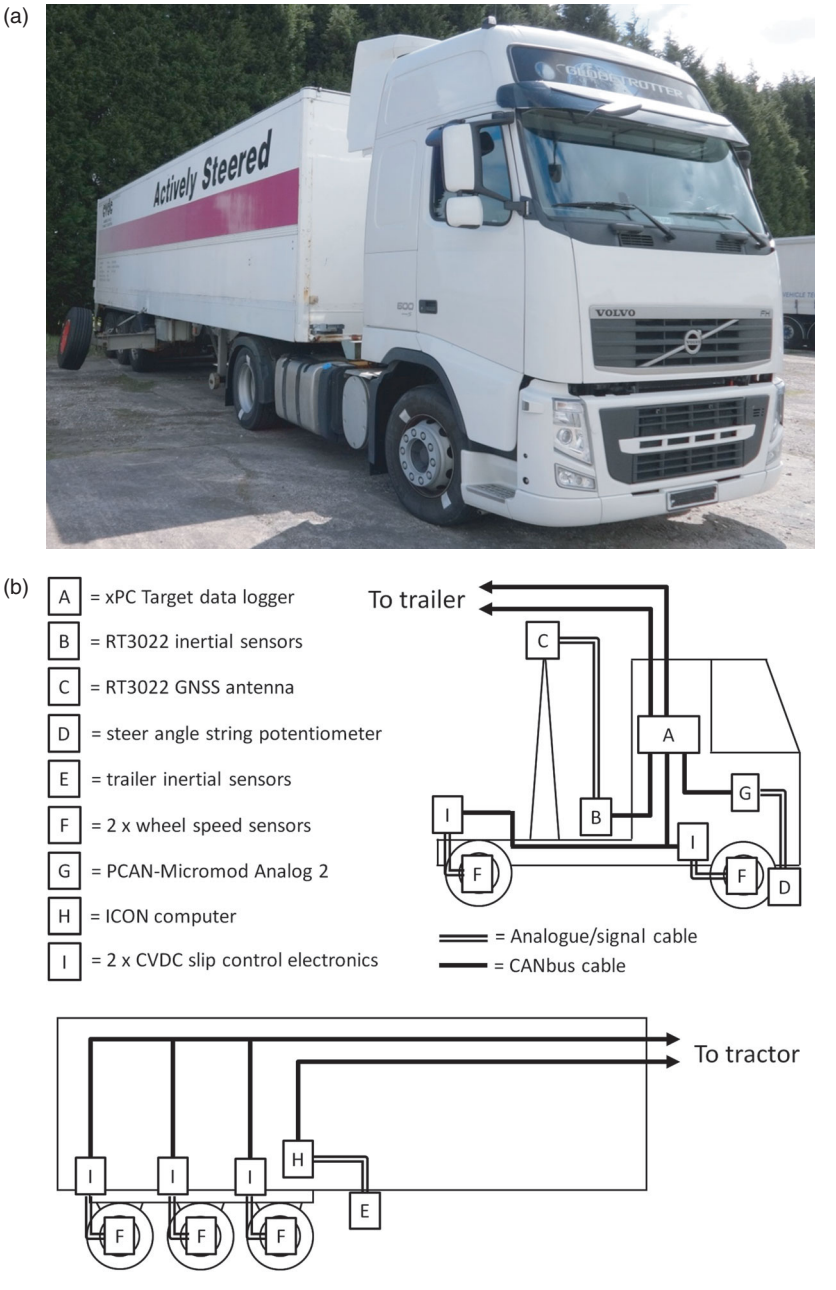

Figure 9. Tractor–semitrailer test vehicle: (a) photograph and (b) schematic of installed instrumentation.

RT3022 was combined with the longitudinal speed measurement to provide a reference sideslip angle signal, to which the observer estimates could be compared.

A string potentiometer was installed between a rigid mounting on the tractor frame and the steering drop-arm. This was calibrated to measure the road–wheel steering angle, which was required as an input to the observers.

The trailer was instrumented with a custom-built six-axis set of inertial sensors, mounted on the trailer frame as close as possible to its CoG, the position of which was determined by weighing the axles. Signals from the lateral accelerometer, yaw gyroscope and roll gyroscope provided the remaining three measurements of trailer lateral acceleration, yaw rate and roll rate required by the observers (see Equation (3)).

Finally, the wheel speeds measured by the CVDC braking system were logged. These were used in combination with the RT3022 vehicle speed measurement to calculate the mean longitudinal wheel slips on each axle, as inputs to the FUKF.

5.2. Test manoeuvres

The following manoeuvres were performed:

(i) 4.4 × 61 m lane change on a dry 'Dunlop Delugrip' surface ($\mu \approx 0.9$), 88 km/h;
(ii) constant 100 m radius corner on a wet basalt tile surface ($\mu \approx 0.15$), 35 km/h;
(iii) 3 × 61 m lane change on a wet basalt tile surface ($\mu \approx 0.12$), 40 km/h.

The manoeuvres on the low-friction wet basalt tile surfaces were performed both at constant speed, and with emergency braking commencing at the point of turn in to the

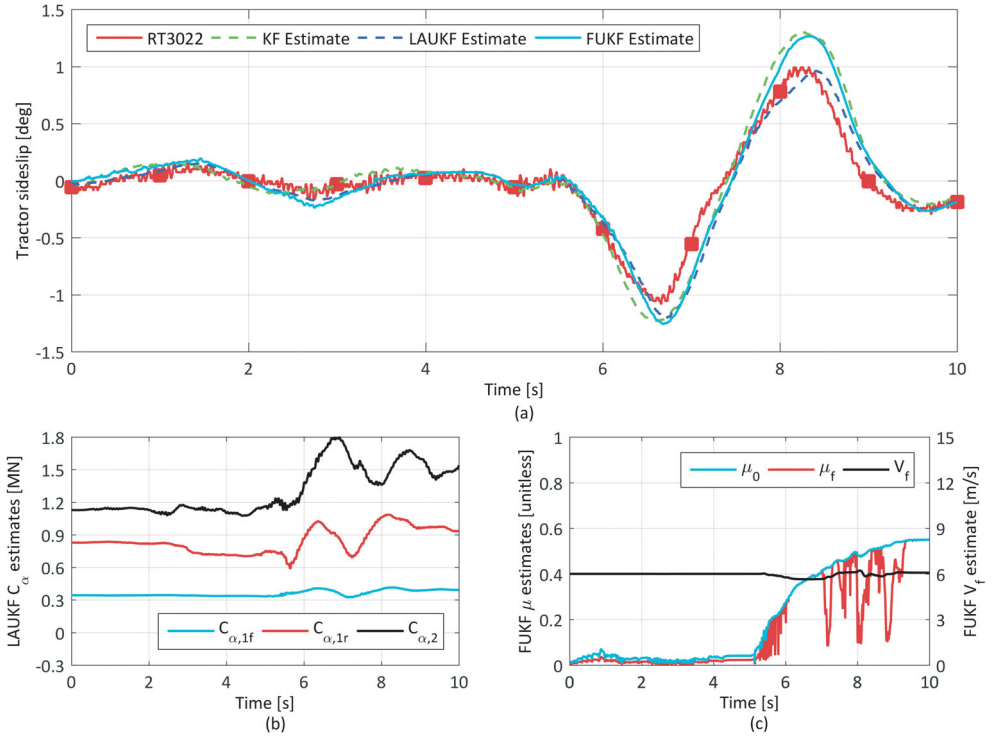

Figure 10. Observer performance on test data from a constant speed lane change manoeuvre on dry Dunlop Delugrip ($\mu \approx 0.9$). Estimated: (a) tractor sideslip; (b) cornering stiffness (LAUKF); and (c) friction parameters (FUKF).

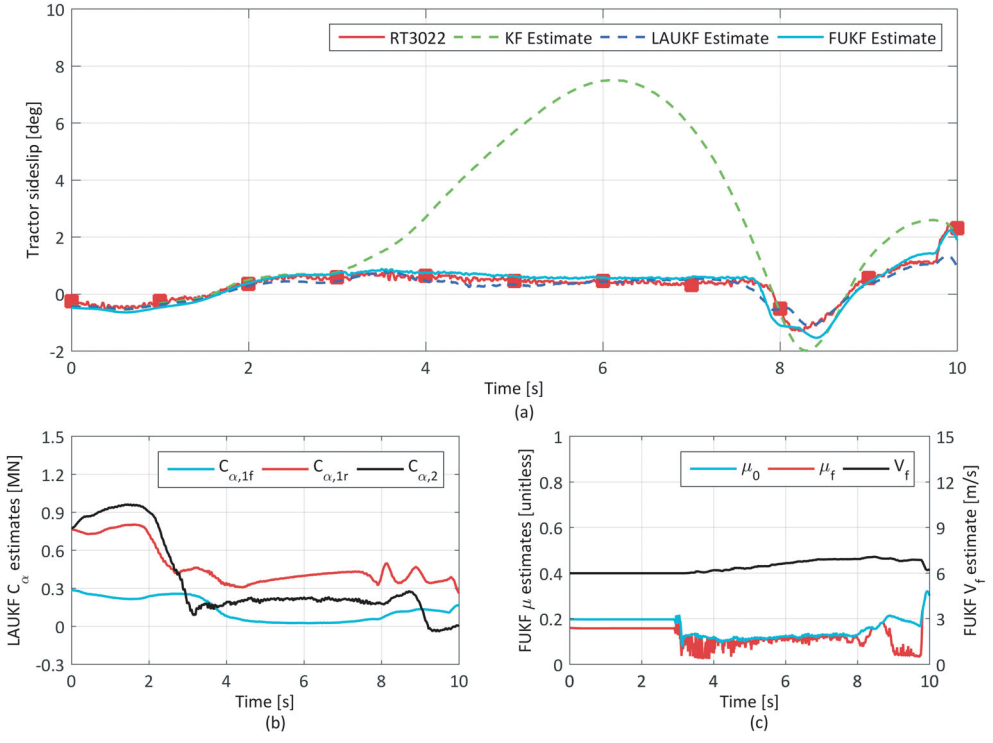

Figure 11. Observer performance on test data from a constant speed, constant radius corner manoeuvre on wet basalt tiles ($\mu \approx 0.15$). Estimated: (a) tractor sideslip; (b) cornering stiffness (LAUKF); and (c) friction parameters (FUKF).

manoeuvre. The manoeuvre on the high-friction Delugrip surface was performed only at constant speed.

5.3. Observer tuning

The measurement noise covariance matrices for each observer were the same as used in the computer simulations in Section 4 (see Appendix 2). The process noise covariance matrices had to be retuned when moving from the simulations to experimental data. These are given in Appendix 2. The tuning for each observer remained the same for all manoeuvres. All of the observers were run with a 100 Hz sampling frequency.

5.4. Constant speed cornering

Figure 10 shows results for the high-friction lane change manoeuvre. With the tyres well below the limits of adhesion, the linear KF gave a reasonably accurate sideslip estimate and the FUKF was similar. However, the LAUKF outperformed both by virtue of making small adjustments to the cornering stiffness estimates to correct any slight mismatch between the observer model and the real vehicle. This significantly reduced the sideslip estimation error near the peak between 8 and 9 s.

Figures 11 and 12 show the constant radius corner and lane change manoeuvres, respectively, on the low-friction surface. Due to operating near the limits of adhesion, the KF

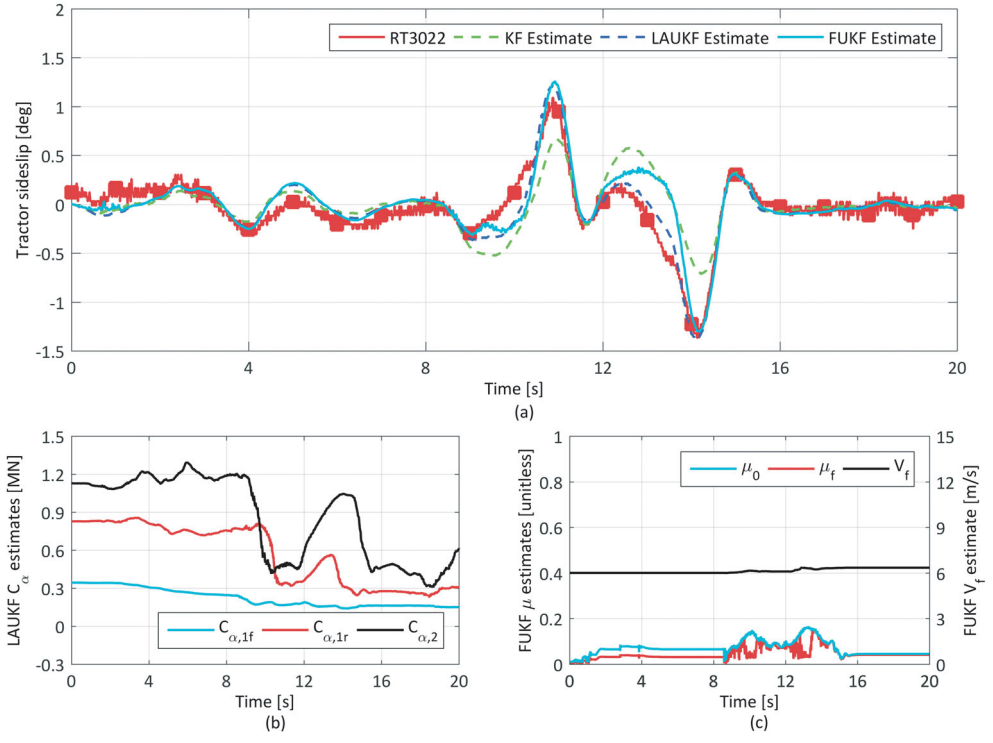

Figure 12. Observer performance on test data from a constant speed lane change manoeuvre on wet basalt tiles ($\mu \approx 0.12$). Estimated: (a) tractor sideslip; (b) cornering stiffness (LAUKF); and (c) friction parameters (FUKF).

performed poorly in both manoeuvres, with up to 7° sideslip error in the constant radius corner. Both the LAUKF and FUKF gave accurate sideslip estimates in the constant radius corner, within around 0.2° for most of the manoeuvre. In the lane change, the LAUKF was again accurate, with a maximum error of just 0.37°. The FUKF gave qualitatively a much better estimate than the KF, accurately picking up the major sideslip peaks and troughs, but could not match the accuracy of the LAUKF throughout the entire manoeuvre and at times gave errors similarly large to the KF. The static friction estimates by the FUKF generally agreed well with the expected values in both manoeuvres, though tended to fluctuate depending on the amount of friction being utilised at any given time.

Table 1 provides a summary of root-mean-squared (RMS) sideslip errors for each observer during the three constant speed manoeuvres. The LAUKF had the lowest error in both lane change manoeuvres and was a close second to the FUKF in the constant radius corner, where the linear KF gave substantially larger errors than both nonlinear observers.

5.5. Emergency braking and cornering

Figure 13 shows results for the constant radius corner manoeuvre on the low-friction surface. With the tyres now operating even further into their nonlinear region due to the heavy braking, the linear KF produced a sideslip estimate with errors of over 12° at times.

Table 1. RMS sideslip estimation errors of Cheng and Cebon's linear KF, LAUKF and nonlinear FUKF when applied to field test data.

		KF RMS error (°)	LAUKF RMS error (°)	FUKF RMS error (°)
Constant speed	Constant radius corner (low μ)	3.29	0.26	0.21
	Lane change (low μ)	0.36	0.14	0.24
	Lane change (high μ)	0.22	0.15	0.19
ASD braking	Constant radius corner (low μ)	1.62	0.98	5.05
	Lane change (low μ)	0.33	0.41	3.30
SC braking	Constant radius corner (low μ)	8.21	1.03	3.01
	Lane change (low μ)	3.68	1.27	0.83

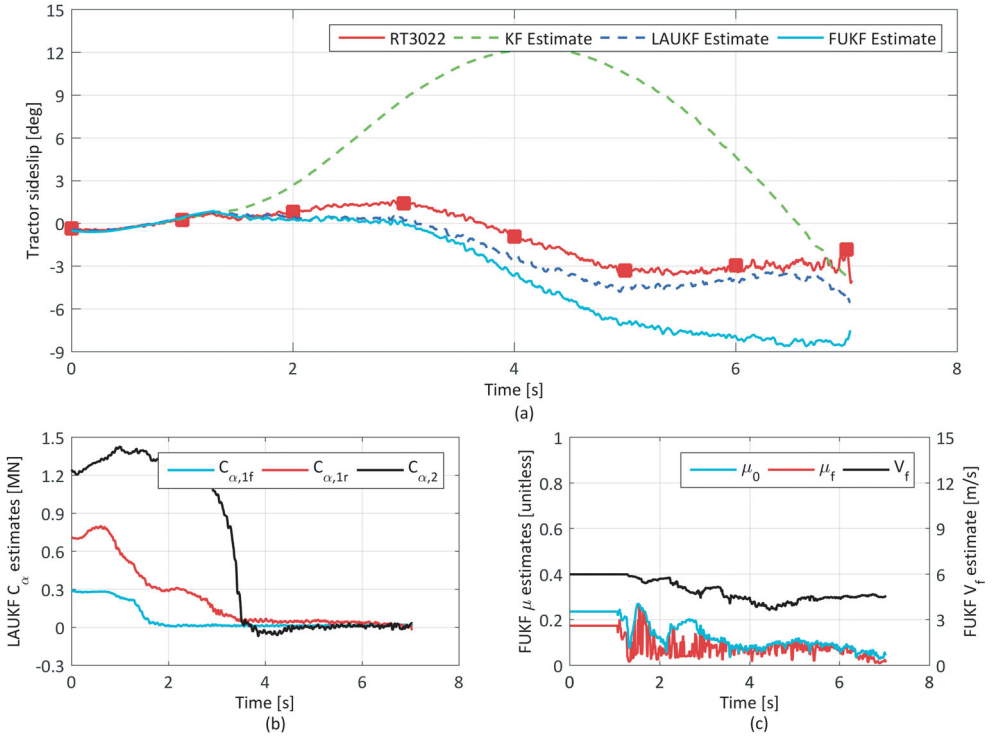

Figure 13. Observer performance on test data from a constant radius corner manoeuvre during emergency braking on wet basalt tiles ($\mu \approx 0.15$). Estimated: (a) tractor sideslip; (b) cornering stiffness (LAUKF); and (c) friction parameters (FUKF).

The FUKF outperformed the linear KF, producing sideslip estimate that was qualitatively similar to the RT3022 measurement, though still with significant quantitative error. Previous work [6] had revealed that when operating with lateral tyre slip only, the Fancher model could simulate the test vehicle's tyre forces on wet basalt tile surfaces with reasonable accuracy. However, significant mismatch between the model and test vehicle was found to occur under combined slip conditions. The level of flexibility afforded to the observer by the three adaptive friction parameters appears to have been insufficient in this scenario to overcome the tyre model mismatch. Alternatively, as postulated in Section 4.2, the FUKF

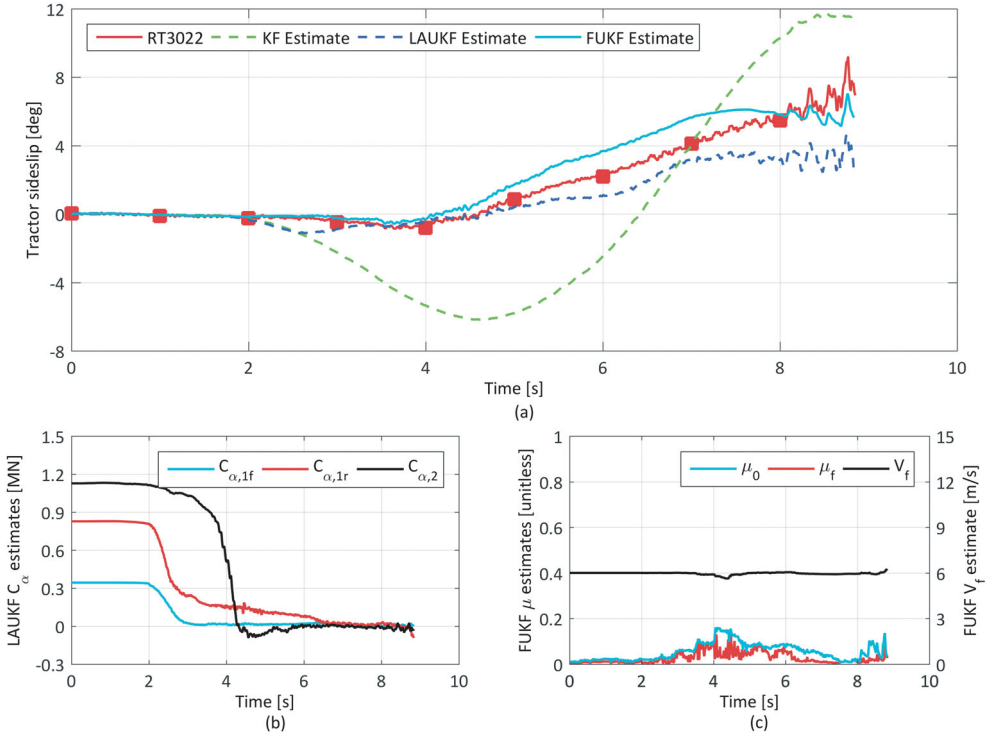

Figure 14. Observer performance on test data from a lane change manoeuvre during emergency braking on wet basalt tiles ($\mu \approx 0.12$). Estimated: (a) tractor sideslip; (b) cornering stiffness (LAUKF); and (c) friction parameters (FUKF).

model might be only weakly observable and therefore was simply unable to correctly adapt the three friction parameters in this scenario.

The LAUKF produced the most accurate estimate of the three observers, with an RMS error of only 1°. Although significantly less accurate than in the constant speed manoeuvres, this was considered a satisfying result given the extremely tough operating conditions created by heavy braking on such a low-friction surface. The cornering stiffness estimates all fell to near zero during the manoeuvre, reflecting how little lateral force the saturated tyres were able to generate. The additional flexibility afforded to the LAUKF by having a single adaptable tyre parameter for each axle, rather than three adaptable friction parameters for the whole vehicle as for the FUKF, appears to give it an advantage when dealing with real tyres with unknown characteristics.

Figure 14 shows the lane change manoeuvre on the low-friction surface. Again the linear KF performed poorly with sideslip errors up to around 7°. Qualitatively, the LAUKF sideslip estimate appears close to the RT3022 measurement, though significant quantitative errors of 3–4° occurred towards the end of the manoeuvre at very low speeds. At such low speeds, the system has very little excitation, creating additional difficulty for the observers. In this manoeuvre, the FUKF slightly outperformed the LAUKF in terms of the magnitude of sideslip errors, though qualitatively the sideslip estimates of the two observers were very similar. The FUKF appears to have been better able to compensate for tyre model mismatch

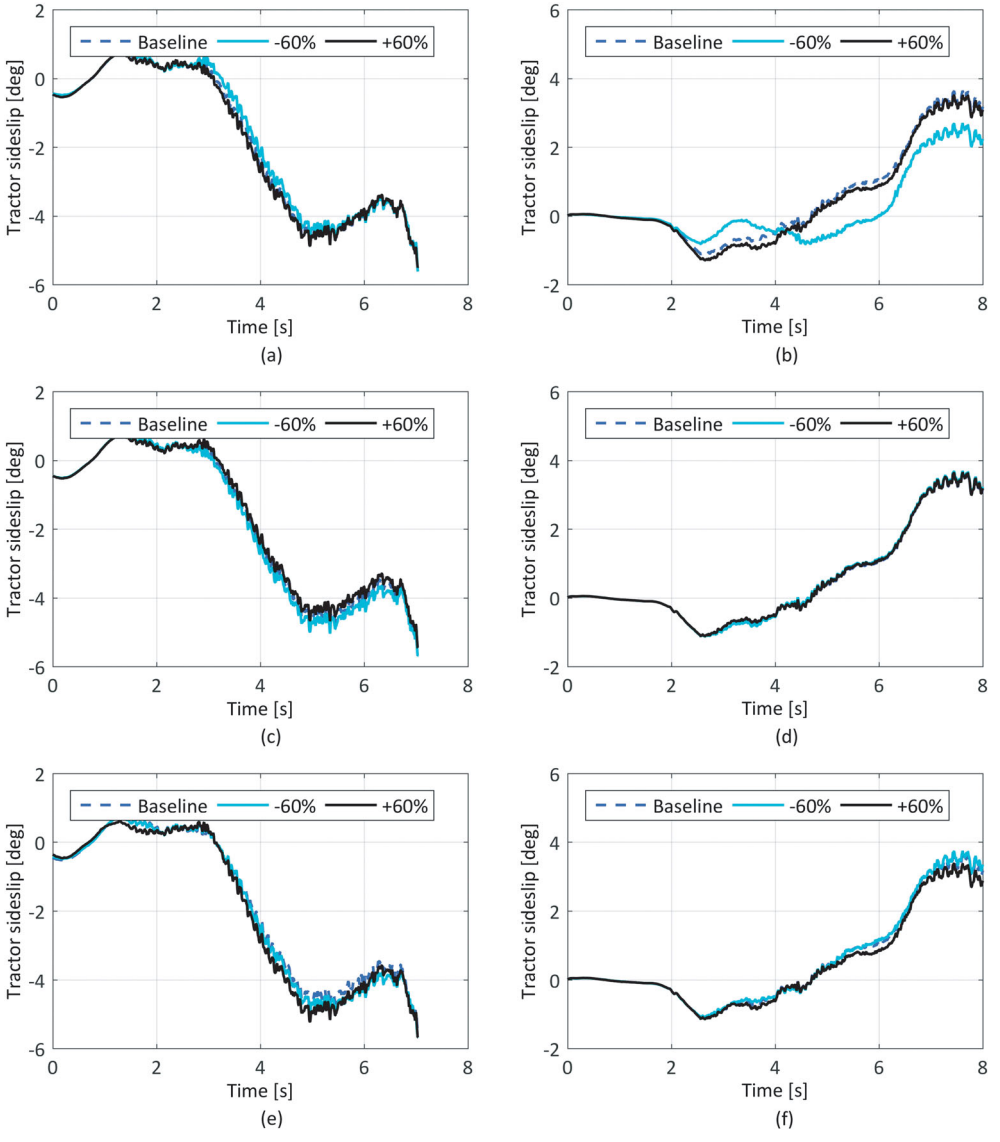

Figure 15. Sensitivity of LAUKF sideslip estimates to parameter variations of ±60%, for emergency braking manoeuvres on wet basalt tiles: (a) effect of trailer yaw moment of inertia, constant radius corner; (b) effect of trailer yaw moment of inertia, lane change; (c) effect of trailer sprung mass roll moment of inertia, constant radius corner; (d) effect of trailer sprung mass roll moment of inertia, lane change; (e) effect of trailer sprung mass CoG height, constant radius corner; and (f) effect of trailer sprung mass CoG height, lane change.

by adapting the friction parameter estimates in this particular manoeuvre, in comparison to the constant radius corner.

Table 1 includes a summary of RMS sideslip errors for each observer during the emergency braking manoeuvres. Only the LAUKF maintained a small error in both manoeuvres, despite being marginally outperformed by the FUKF in the lane change.

6. Parameter sensitivity

Many of the vehicle parameters required for the observers can be accurately measured or estimated, and would not change significantly during day-to-day HGV operation. However, there are some exceptions, particularly relating to the trailer loading condition. Trailer mass and longitudinal CoG location can be reasonably calculated online, from the estimates of static axle weights (based on air suspension pressures) which are typically available on modern HGVs.[43] However, the yaw and roll moments of inertia and CoG height of the trailer are more difficult to know with certainty.

The sensitivity of the LAUKF to large errors in these three parameters was investigated. The LAUKF appeared to be the most consistently accurate and reliable observer when applied to the experimental data. It should also be robust to errors in the nominal cornering stiffness parameters, since it adapts them as part of the estimation process.

The LAUKF was applied to the combined emergency braking and cornering test data (as per Figures 13 and 14), with the trailer yaw moment of inertia, trailer roll moment of inertia and trailer CoG height parameters varied individually by $\pm 60\%$ from their nominal values. Figure 15 shows the sideslip estimation results with each parameter variation in both the constant radius corner and lane change manoeuvres with emergency braking, in comparison to when using the nominal parameter set. The LAUKF appears to be remarkably insensitive to such large variations. The greatest sensitivity was to a reduction in trailer yaw moment of inertia, but even in this case the sensitivity is low given the large parameter variation. Therefore, it should be robust to uncertain trailer loading conditions during service.

7. Conclusions

This paper investigated three nonlinear observers for HGV sideslip estimation, in an attempt to improve on the state-of-the-art linear KF.[44] LAEKF, LAUKF and FUKF were considered. Each of these three nonlinear observers were based around the same underlying vehicle model as Cheng and Cebon's KF, but augmented with either an adaptive or nonlinear tyre model in order to improve performance at the limits of tyre adhesion.

Simulations suggested that the LAUKF and FUKF had potential to substantially outperform the linear KF, particularly in low-friction conditions. Despite utilising exactly the same vehicle and tyre models as the LAUKF, the LAEKF performed poorly on low-friction surfaces due to the linearisation of the observer model by the EKF. Eigenvalue decomposition and limiting of the state estimate covariance matrix were demonstrated for the LAUKF, to fix a divergence problem observed at times of low vehicle excitation.

The linear KF, LAUKF and FUKF were further tested on experimental data from a full-scale tractor–semitrailer. The LAUKF generally performed well across all of the test scenarios, substantially outperforming the linear KF. The FUKF matched the performance of the linear KF in a high-friction lane change manoeuvre and outperformed the linear KF in all of the low-friction scenarios. However, large errors could occur under combined slip conditions where the Fancher tyre model was known not to match the tyres of the test vehicle well. The LAUKF appeared to have greater flexibility to deal unknown real tyre characteristics. Future work should consider whether the Fancher tyre model

can be improved for combined slip conditions or substituted for an alternative nonlinear tyre model, in order to replicate the promising simulation results of the FUKF with experimental data.

Finally, the sensitivity of the LAUKF to those vehicle parameters most heavily influenced by trailer loading condition was considered. The LAUKF showed very little sensitivity to even large (±60%) variations in the most uncertain parameters, therefore should be robust to varying trailer loads during service.

Acknowledgements

The authors would like to thank Volvo Trucks and Anthony Best Dynamics for the provision of test equipment; HORIBA MIRA for the provision of test tracks; Haldex Brake Products and Dr Leon Henderson (previously University of Cambridge, now Chalmers University of Technology) for their technical assistance during field testing.

Disclosure statement

No potential conflict of interest was reported by the authors.

Funding

This work was funded by the Engineering and Physical Sciences Research Council and the Cambridge Vehicle Dynamics Consortium (CVDC). At the time of writing, the members of the CVDC included Anthony Best Dynamics, Camcon, Denby Transport, Firestone, Goodyear, Haldex, SIMPACK, HORIBA MIRA, SDC Trailers, Tinsley Bridge, Tridec, Volvo Trucks and Wincanton.

References

[1] Cheng C, Roebuck R, Odhams A, Cebon D. High-speed optimal steering of a tractor–semitrailer. Vehicle Syst Dyn. 2011;49(4):561–593.
[2] Cheng C, Cebon D. Improving roll stability of articulated heavy vehicles using active semitrailer steering. Vehicle Syst Dyn. 2008;46(Suppl 1):373–388.
[3] Jujnovich BA, Cebon D. Path-following steering control for articulated vehicles. J Dyn Syst Meas Control. 2013;135(3):031006(1–15).
[4] Palkovics L, El-Gindy M. Design of an active unilateral brake control system for five-axle tractor–semitrailer based on sensitivity analysis. Vehicle Syst Dyn. 1995;24(10):725–758.
[5] Eisele D, Peng H. Vehicle dynamics control with rollover prevention for articulated heavy trucks. Paper presented at: 5th International Symposium on Advanced Vehicle Control; 2000; MI, USA.
[6] Morrison G. Combined emergency braking and cornering of articulated heavy vehicles [PhD dissertation]. Cambridge: Department of Engineering, University of Cambridge; 2015.
[7] Morrison G, Cebon D. Field testing of control strategies for combined emergency braking and turning of articulated heavy vehicles. J Dyn Syst Meas Control. 2016.
[8] Morrison G, Cebon D. Combined emergency braking and turning of articulated heavy vehicles. Vehicle Syst Dyn. 2016.
[9] Kiencke U, Daiß A. Observation of lateral vehicle dynamics. Control Eng Pract. 1997;5(8):1145–1150.
[10] Dixon PJ, Best MC, Gordon TJ. An extended adaptive Kalman filter for real-time state estimation of vehicle handling dynamics. Vehicle Syst Dyn. 2000;34(1):57–75.
[11] Dakhlallah J, Glaser S, Mammar S, Sebsadji Y. Tire-road forces estimation using extended Kalman filter and sideslip angle evaluation. Paper presented at: American Control Conference; 2008; WA, USA.

[12] Baffet G, Charara A, Stephant J. Sideslip angle, lateral tire force and road friction estimation in simulations and experiments. Paper presented at: IEEE International Symposium on Intelligent Control; 2006; Munich, Germany.
[13] Hac A, Simpson MD. Estimation of vehicle side slip angle and yaw rate. SAE Technical Paper 2000-01-0696; 2000.
[14] Sasaki H, Nishimaki T. A side-slip angle estimation using neural network for a wheeled vehicle. SAE Technical Paper 2000-01-0695; 2000.
[15] Stephant J, Charara A, Meizel D. Evaluation of a sliding mode observer for vehicle sideslip angle. Control Eng Pract. 2007;15(7):803–812.
[16] Ungoren AY, Peng H. A study on lateral speed estimation methods. Int J Vehicle Auton Syst. 2002;1(1):126–144.
[17] Farrelly J, Wellstead P. Estimation of vehicle lateral velocity. Paper presented at: IEEE International Conference on Control Applications; 1996; MI, USA.
[18] Chen B, Hsieh F. Sideslip angle estimation using extended Kalman filter. Vehicle Syst Dyn. 2008;46(Suppl 1):353–364.
[19] Cheng C, Cebon D. Parameter and state estimation for articulated heavy vehicles. Vehicle Syst Dyn. 2010;49(1–2):399–418.
[20] Morrison G, Cebon D. Sideslip estimation for articulated heavy vehicles in low friction conditions. Paper presented at: IEEE Intelligent Vehicles Symposium; 2015; Seoul, Korea.
[21] Ma Z, Zhang Y, Yang J. Velocity and normal tyre force estimation for heavy trucks based on vehicle dynamic simulation considering the road slope angle. Vehicle Syst Dyn. 2016;54(2):137–167.
[22] Julier SJ, Uhlmann JK. Unscented filtering and nonlinear estimation. Proc IEEE. 2004;92(3):401–422.
[23] Van Der Merwe R, Wan EA. Sigma-point Kalman filters for integrated navigation. Paper presented at: Proceedings of the 60th Annual Meeting of the Institute of Navigation; 2004; OH, USA.
[24] Julier SJ, Uhlmann JK. A new extension of the Kalman filter to nonlinear systems. Paper presented at: International Symposium of Aerospace/Defense Sensing, Simulation and Controls; 1997; FL, USA.
[25] Wan EA, Van Der Merwe R. The unscented Kalman filter for nonlinear estimation. Paper presented at: IEEE Adaptive Systems for Signal Processing, Communications, and Control Symposium; 2000; Alberta, Canada.
[26] Antonov S, Fehn A, Kugi A. Unscented Kalman filter for vehicle state estimation. Vehicle Syst Dyn. 2011;49(9):1497–1520.
[27] Fancher P. Generic data for representing truck tire characteristics in simulations of braking and braking-in-a-turn maneuvers. MI, USA: UMTRI; 1995. (UMTRI 95-34).
[28] Cheng C. Enhancing safety of actively-steered articulated vehicles [PhD dissertation]. Cambridge: Department of Engineering, University of Cambridge; 2009.
[29] Stenlund B, Gustafsson F. Avoiding windup in recursive parameter estimation. Paper presented at: Reglermöte; 2002; Linköping, Sweden.
[30] Parkum JE, Poulsen NK, Holst J. Recursive forgetting algorithms. Int J Control. 1992;55(1):109–128.
[31] Liyu C, Schwartz HM. A novel recursive algorithm for directional forgetting. Paper presented at: American Control Conference; 1999; CA, USA.
[32] Andersson A, Broman H. A second-order recursive algorithm with applications to adaptive filtering and subspace tracking. IEEE Trans Signal Process. 1998;46(6):1720–1725.
[33] Gunnarsson S. Combining tracking and regularization in recursive least squares identification. Paper presented at: IEEE Conference on Decision and Control; 1996; Kobe, Japan.
[34] Hägglund T. New estimation techniques for adaptive control [PhD dissertation]. Lund: Department of Automatic Control, Lund University; 1983.
[35] Henderson L, Cebon D. Full-scale testing of a novel slip control braking system for heavy vehicles. Proc IMechE D: J Automobile Eng. doi:10.1177/0954407015604804. Published Online Before Print, September 2015.

[36] Henderson L. Improving emergency braking performance of heavy goods vehicles [PhD dissertation]. Cambridge: Department of Engineering, University of Cambridge; 2013.
[37] Bevly DM, Parkinson B. Cascaded Kalman filters for accurate estimation of multiple biases, dead-reckoning navigation, and full state feedback control of ground vehicles. IEEE Trans Contr Syst T. 2007;15(2):199–208.
[38] Kimbrough S, Datla K. An effective means for implementing wheelslip control without a ground speed sensor. Vehicle Syst Dyn. 1996;25(Suppl):327–339.
[39] Bowman JE, Law E. A feasibility study of an automotive slip control braking system. SAE Technical Paper 930762; 1993.
[40] Watanabe K, Kinase K, Kobayashi K. Absolute speed measurement of automobile from noisy acceleration and erroneous wheel speed information. SAE Technical Paper 920644; 1992.
[41] Jiang F, Gao Z. An adaptive nonlinear filter approach to the vehicle velocity estimation for ABS. Paper presented at: IEEE International Conference on Control Applications; 2000; AK, USA.
[42] Kienhöfer F. Heavy vehicle wheel slip control [PhD dissertation]. Cambridge: Department of Engineering, University of Cambridge; 2006.
[43] HDEI/BCEI Working Group. FMS-standard description version 03. 2012. Available from: http://www.fms-standard.com/
[44] Miller J, Henderson LM, Cebon D. Designing and testing an advanced pneumatic braking system for heavy vehicles. Proc IMechE C: J Mech Eng Sci. 2012;227(8):1715–1729.

Appendix 1. 5 DoF yaw–roll model

$$\boldsymbol{A}(u_1) = \boldsymbol{M}^{-1}\boldsymbol{S} \qquad \boldsymbol{B}(u_1) = \boldsymbol{M}^{-1}\boldsymbol{E} \qquad \boldsymbol{C}(u_1) = \boldsymbol{V}\boldsymbol{A} + \boldsymbol{W} \qquad \boldsymbol{D}(u_1) = \boldsymbol{V}\boldsymbol{B},$$

where

$$\boldsymbol{M} = \begin{bmatrix} 0 & -(I_{1sxz} + m_{1s}l_{1c}h_{1sr}) & m_1 l_{1c} u_1 & I_{1zz} \\ 0 & I_{1sxx} + m_{1s}h_{1sr}(h_{1sr} - h_{1cr}) & (m_1 h_{1cr} - m_{1s}h_{1sr})u_1 & -I_{1sxz} \\ 0 & -m_{1s}h_{1sr} & m_1 u_1 & 0 \\ 0 & 0 & 0 & 0 \\ 0 & 0 & 0 & 0 \\ 0 & h_{1cr}/u_1 & -1 & l_{1c}/u_1 \\ 1 & 0 & 0 & 0 \\ 0 & 0 & 0 & 0 \end{bmatrix}$$

$$\begin{bmatrix} 0 & 0 & 0 & 0 \\ 0 & 0 & 0 & 0 \\ 0 & -m_{2s}h_{2sr} & m_2 u_1 & 0 \\ 0 & -(I_{2sxz} - m_{2s}l_{2c}h_{2sr}) & -m_2 l_{2c} u_1 & I_{2zz} \\ 0 & I_{2sxx} + m_{2s}h_{2sr}(h_{2sr} - h_{2cr}) & (m_2 h_{2cr} - m_{2s}h_{2sr})u_1 & -I_{2sxz} \\ 0 & -h_{2cr}/u_1 & 1 & l_{2c}/u_1 \\ 0 & 0 & 0 & 0 \\ 1 & 0 & 0 & 0 \end{bmatrix}$$

$$\boldsymbol{S} = \frac{1}{u_1}\begin{bmatrix} 0 & 0 & (l_{1r}C_{\alpha,1r} - l_{1f}C_{\alpha,1f} - (C_{\alpha,1f} + C_{\alpha,1r})l_{1c})u_1 \\ (m_{1s}gh_{1sr} - K_1^* - K_{12})u_1 & -C_1^* u_1 & -h_{1cr}(C_{\alpha,1f} + C_{\alpha,1r})u_1 \\ 0 & 0 & -(C_{\alpha,1f} + C_{\alpha,1r})u_1 \\ 0 & 0 & 0 \\ K_{12}u_1 & 0 & 0 \\ 0 & 0 & 0 \\ 0 & u_1 & 0 \\ 0 & 0 & 0 \end{bmatrix}$$

$$\begin{bmatrix} l_{1c}(l_{1r}C_{\alpha,1r} - l_{1f}C_{\alpha,1f} - m_1u_1^2) - (l_{1f}^2C_{\alpha,1f} + l_{1r}^2C_{\alpha,1r}) & 0 \\ h_{1cr}(l_{1r}C_{\alpha,1r} - l_{1f}C_{\alpha,1f} - m_1u_1^2) + m_{1s}u_1^2h_{1sr} & K_{12}u_1 \\ (l_{1r}C_{\alpha,1r} - l_{1f}C_{\alpha,1f} - m_1u_1^2) & 0 \\ 0 & 0 \\ 0 & (m_{2s}gh_{2sr} - K_2^* - K_{12})u_1 \\ u_1 & 0 \\ 0 & 0 \\ 0 & 0 \end{bmatrix}$$

$$\begin{bmatrix} 0 & 0 & 0 \\ 0 & 0 & 0 \\ 0 & -C_{\alpha,2}u_1 & l_{2r}C_{\alpha,2} - m_2u_1^2 \\ 0 & (l_{2r} + l_{2c})C_{\alpha,2}u_1 & m_2u_1^2l_{2c} - (l_{2r}^2 + l_{2r}l_{2c} + 2l_{2aa}/3)C_{\alpha,2} \\ -C_2^*u_1 & -h_{2cr}C_{\alpha,2}u_1 & h_{2cr}(l_{2r}C_{\alpha,2} - m_2u_1^2) + m_{2s}u_1^2h_{2sr} \\ 0 & 0 & -u_1 \\ 0 & 0 & 0 \\ u_1 & 0 & 0 \end{bmatrix}$$

$$\boldsymbol{E} = \begin{bmatrix} (l_{1c} + l_{1f})C_{\alpha,1f} \\ h_{1cr}C_{\alpha,1f} \\ C_{\alpha,1f} \\ 0 \\ 0 \\ 0 \\ 0 \\ 0 \end{bmatrix}, \quad \boldsymbol{V} = \begin{bmatrix} 0 & -h_{1sr}m_{1s}/m_1 & u_1 & 0 & 0 & 0 & 0 & 0 \\ 0 & 0 & 0 & 0 & 0 & 0 & 0 & 0 \\ 0 & 0 & 0 & 0 & 0 & 0 & 0 & 0 \\ 0 & 0 & 0 & 0 & 0 & -h_{2sr}m_{2s}/m_2 & u_1 & 0 \\ 0 & 0 & 0 & 0 & 0 & 0 & 0 & 0 \\ 0 & 0 & 0 & 0 & 0 & 0 & 0 & 0 \end{bmatrix}$$

$$\boldsymbol{W} = \begin{bmatrix} -g & 0 & 0 & u_1 & 0 & 0 & 0 & 0 \\ 0 & 0 & 0 & 1 & 0 & 0 & 0 & 0 \\ 0 & 1 & 0 & 0 & 0 & 0 & 0 & 0 \\ 0 & 0 & 0 & 0 & -g & 0 & 0 & u_1 \\ 0 & 0 & 0 & 0 & 0 & 0 & 0 & 1 \\ 0 & 0 & 0 & 0 & 0 & 1 & 0 & 0 \end{bmatrix}$$

Appendix 2. Covariance parameters

Measurement noise covariance matrix for all observers:

$$\boldsymbol{R} = \text{diag}([0.096 \quad 1.5 \times 10^{-5} \quad 4.5 \times 10^{-4} \quad 0.049 \quad 1.1 \times 10^{-5} \quad 4.7 \times 10^{-5}])$$
$$\text{units: } [(\text{m/s}^2)^2 \quad (\text{rad/s})^2 \quad (\text{rad/s})^2 \quad (\text{m/s}^2)^2 \quad (\text{rad/s})^2 \quad (\text{rad/s})^2]$$

State estimate covariance matrices in simulations:

$$\boldsymbol{Q_{KF}} = \text{diag}\left([10^{-4} \quad 10^{-4} \quad 10^{-4} \quad 10^{-4} \quad 10^{-4} \quad 10^{-4} \quad 10^{-4} \quad 10^{-4}]\right)$$
$$\text{units: } [(\text{rad})^2 \ (\text{rad/s})^2 \ (\text{rad})^2 \ (\text{rad/s})^2 \ (\text{rad})^2 \ (\text{rad/s})^2 \ (\text{rad})^2 \ (\text{rad/s})^2]$$

$$\boldsymbol{Q_{LAEKF}} = \boldsymbol{Q_{LAUKF}}$$
$$= \text{diag}([10^{-6} \quad 10^{-6} \quad 10^{-6} \quad 10^{-3} \quad 10^{-6} \quad 10^{-6} \quad 10^{-6} \quad 10^{-3}$$
$$C_{\alpha(0),1f}^2 \quad C_{\alpha(0),1r}^2 \quad C_{\alpha(0),2}^2])$$
$$\text{units: } [(\text{rad})^2(\text{rad/s})^2(\text{rad})^2(\text{rad/s})^2(\text{rad})^2(\text{rad/s})^2(\text{rad})^2(\text{rad/s})^2(\text{N})^2(\text{N})^2(\text{N})^2]$$

$$\boldsymbol{Q_{FUKF}} = \text{diag}([10^{-6} \quad 10^{-6} \quad 10^{-6} \quad 10^{-3} \quad 10^{-6} \quad 10^{-6} \quad 10^{-6} \quad 10^{-3} \quad 10^{-1} \quad 10^{2} \quad 10])$$

$$\text{units: } [(\text{rad})^2(\text{rad/s})^2(\text{rad})^2(\text{rad/s})^2(\text{rad})^2(\text{rad/s})^2(\text{rad})^2(\text{rad/s})^2 \\ (\text{unitless})(\text{unitless})(\text{m/s})^2]$$

State estimate covariance matrices in experiments:

$$\boldsymbol{Q_{KF}} = \text{diag}([10^{-4} \quad 10^{-4} \quad 10^{-4} \quad 10^{-4} \quad 10^{-4} \quad 10^{-4} \quad 10^{-4} \quad 10^{-4}])$$

$$\text{units: } [(\text{rad})^2(\text{rad/s})^2(\text{rad})^2(\text{rad/s})^2(\text{rad})^2(\text{rad/s})^2(\text{rad})^2(\text{rad/s})^2]$$

$$\boldsymbol{Q_{LAUKF}} = \text{diag}([10^{-6} \quad 10^{-6} \quad 10^{-6} \quad 2 \times 10^{-2} \quad 10^{-6} \quad 10^{-6} \quad 10^{-6} \quad 2 \times 10^{-2} \quad \cdots \\ C^2_{\alpha(0),1\text{f}}/14 \quad C^2_{\alpha(0),1\text{r}}/6 \quad C^2_{\alpha(0),2}/4])$$

$$\text{units: } [(\text{rad})^2(\text{rad/s})^2(\text{rad})^2(\text{rad/s})^2(\text{rad})^2(\text{rad/s})^2(\text{rad})^2(\text{rad/s})^2(N)^2(N)^2(N)^2]$$

$$\boldsymbol{Q_{FUKF}} = \text{diag}([10^{-6} \quad 10^{-6} \quad 10^{-6} \quad 2 \times 10^{-2} \quad 10^{-6} \quad 10^{-6} \quad 10^{-6} \quad 2 \times 10^{-2} \\ 10^{-1} \quad 10^{2} \quad 10 \ ])$$

$$\text{units: } [(\text{rad})^2(\text{rad/s})^2(\text{rad})^2(\text{rad/s})^2(\text{rad})^2(\text{rad/s})^2(\text{rad})^2(\text{rad/s})^2 \\ (\text{unitless})(\text{unitless})(\text{m/s})^2]$$